N86-27195

A DIRECT AND INVERSE BOUNDARY LAYER METHOD FOR SUBSONIC FLOW OVER DELTA WINGS*

Shawn H. Woodson and Fred R. DeJarnette
North Carolina State University
Raleigh, North Carolina

SUMMARY

A new inverse boundary layer method is developed and applied to incompressible flows with laminar separation and reattachment. Test cases for two-dimensional flows are computed and the results are compared with those of other inverse methods. One advantage of the present method is that the calculation of the inviscid velocities may be determined at each marching step without having to iterate.

The inverse method was incorporated with the direct method to calculate the incompressible, conical flow over a slender delta wing at incidence. The location of the secondary separation line on the leeward surface of the wing is determined and compared with experiment for a unit aspect ratio wing at 20.5 deg incidence. The viscous flow in the separated region was calculated using prescribed skin-friction coefficients.

INTRODUCTION

The flow field over slender, highly swept delta wings at moderate incidence is dominated by the presence of large counter-rotating, leading-edge vortices as shown in fig. 1. As the flow moves spanwise towards the leading edge, the adverse pressure gradient caused by the leading-edge vortices causes the boundary layer to separate along a secondary separation line, indicated in fig. 2.

A direct boundary layer method (one in which the external pressure is prescribed from an inviscid calculation or experiment) may be used to determine the location of the secondary separation line (ref. 1). However, in order to continue the solution from the secondary separation line to the leading-edge using boundary layer theory, an inverse method (one in which the wall shear or displacement thickness is specified) must be employed.

Inverse methods have been used by numerous authors since the early work of Catherall and Mangler (ref. 2). Catherall and Mangler used a prescribed displacement thickness distribution to drive a boundary layer method in which the external pressure was determined as part of the solution. In this manner, they were able to obtain a regular solution at separation. However, their numerical scheme developed instabilities in the reversed flow region and the integration was continued only by reducing the convergence criteria at each marching step. This problem of reversed-flow velocity profiles led directly to the FLARE approximation of Reyhner and Flugge-Lotz (ref. 3). In the FLARE approximation the streamwise

* Research supported by NASA Langley Cooperative agreement NCCI-22.

convection of momentum is set equal to zero in the reversed flow region and the calculations proceed with the usual forward marching procedure.

For two-dimensional flows, Klineberg and Steger (ref. 4), Carter (ref. 5) and Cebeci et al. (ref. 6) have developed globally iterative schemes for flows with separation and reattachment. In those methods either the wall shear or displacement thickness is specified and the pressure is obtained iteratively using successive-under-relaxation schemes. Semi-inverse methods have been developed for interacting an inverse boundary layer method with an inviscid solution by Le Balleur (ref. 7), Carter (ref. 8), Kwon and Pletcher (ref. 9) and Veldman (ref. 10) among others. In these methods, the inviscid calculation proceeds in the direct manner with the viscous calculation performed in the inverse mode. Thus, an edge velocity is determined in both calculations which must be the same after convergence.

In three-dimensional flow calculations, several possible combinations of the viscous parameters could be used to drive an inverse method (e.g., CFX, CFY or DTX, DTY). However, Edwards and Carter (ref. 11) have shown that specifying the three-dimensional displacement surface and the component of vorticity normal to the surface leads to an elliptic set of equations and departure solutions for forward marching schemes.

In this paper, a new inverse boundary layer method is developed for separated flows. The method is non-iterative based on a predictor-corrector linearization of the discretized governing equations. For two-dimensional flows, the new method is used to compute the test case of Klineberg and Steger (ref. 4) for a specified wall shear and that of Carter (ref. 5) for the displacement thickness prescribed. The method is also applied to the incompressible, conical, laminar boundary layer flow on the leeward surface of a slender delta wing at incidence. The inviscid solution for the delta wing is determined using the Free Vortex Sheet (FVS) code which was orginally developed at Boeing (ref. 12) and significantly enhanced by Luckring and others (refs. 13, 14) at NASA Langley. The viscous solution for the delta wing is determined in the direct mode until the secondary separation line is encountered (CFY $\leq$ 0), then the calculations are continued in the inverse mode to the leading edge by specifying the skin-friction coefficients to be constant and equal to their values at separation (CFX $>$ 0, CFY $\leq$ 0). The calculations are performed on a unit aspect ratio wing at 20.5 deg incidence which corresponds to the experiment of Hummel (ref. 15).

ANALYSIS

Governing Equations

For steady, incompressible flows, the three-dimensional laminar boundary layer equations in non-dimensional Cartesian coordinates are:

$$\frac{\partial u}{\partial x} + \frac{\partial v}{\partial y} + \frac{\partial w}{\partial z} = 0 \tag{1}$$

$$u \frac{\partial u}{\partial x} + v \frac{\partial u}{\partial y} + w \frac{\partial u}{\partial z} = u_e \frac{\partial u_e}{\partial x} + v_e \frac{\partial u_e}{\partial y} + \frac{\partial^2 u}{\partial z^2} \tag{2}$$

$$u \frac{\partial v}{\partial x} + v \frac{\partial v}{\partial y} + w \frac{\partial v}{\partial z} = u_e \frac{\partial v_e}{\partial x} + v_e \frac{\partial v_e}{\partial y} + \frac{\partial^2 v}{\partial z^2} \tag{3}$$

The velocity components u, v, and w are in the x, y, and z-directions, respectively, where x is in the streamwise direction, y is spanwise and z is normal to the x-y plane. The Reynolds number has been removed from eqs. (1)-(3) by defining $x = \bar{x}/\bar{L}$, $y = \bar{y}/\bar{L}$, $z = \sqrt{Re}\ \bar{z}/\bar{L}$, $u = \bar{u}/\bar{U}_o$, $v = \bar{v}/\bar{U}_o$ and $w = \sqrt{Re}\ \bar{w}/\bar{U}_o$. The superscript bars indicate dimensional quantities and $Re = \bar{U}_o\bar{L}/\bar{\nu}$. The complete derivation of eqs. (1)-(3) is provided in reference 16. The boundary conditions on eqs. (1)-(3) are:

$$\text{at } z = 0 : \quad u = v = w = 0$$

$$\text{and as } z \to \infty : \quad u \to u_e, \quad v \to v_e \tag{4}$$

Two-dimensional Flow

For two-dimensional flow, v = 0 and eqs. (1) and (3) are transformed by defining,

$$X = x \qquad \eta = \left(\frac{u_e}{x}\right)^{1/2} z \tag{5}$$

along with a stream function, ψ, where

$$u = \frac{\partial \psi}{\partial z} \quad \text{and} \quad w = -\frac{\partial \psi}{\partial x} \tag{6}$$

Define a parameter f, such that

$$\psi = (U_e X)^{1/2} f \tag{7}$$

Using eqs. (5) and (7) in eq. (6) yields,

$$\frac{u}{u_e} = \frac{\partial f}{\partial \eta} = F(\eta) \tag{8}$$

With eqs. (5)-(8), eq. (2) may be written as,

$$\frac{\partial^2 F}{\partial \eta^2} + \frac{\partial F}{\partial \eta}\left[X \frac{\partial f}{\partial X} + \left(\frac{m+1}{2}\right) f \right] + m(1-f^2) = XF \frac{\partial F}{\partial X} \tag{9}$$

where $$m = \frac{X}{u_e} \frac{du_e}{dX} \tag{10}$$

The boundary conditions for eq. (9) are

$$\eta = 0 : \quad f = F = 0 , \quad \eta = \eta_e : \quad F = 1.0 \tag{11}$$

Conical Flow Over Delta Wings

For the delta wing a body-oriented coordinate system is defined through the transformation,

$$X = x , \quad Y = (y/x)\tan \Lambda , \quad Z = z/x \tag{12}$$

where Λ is the sweep angle of the delta wing. Define transformed velocity components by,

$$U = u , \quad V = v \tan \Lambda - uY , \quad W = w - uZ \tag{13}$$

Using eqs. (12) and (13) in eq. (1) it becomes,

$$\frac{\partial}{\partial X}(X^2 U) + \frac{\partial}{\partial Y}(XV) + \frac{\partial}{\partial Z}(XW) = 0 \tag{14}$$

Next define two stream functins, ψ and ϕ as

$$X^2 U = \frac{\partial \psi}{\partial Z} , \quad XV = \frac{\partial \phi}{\partial Z} , \quad XW = -\frac{\partial \psi}{\partial X} - \frac{\partial \phi}{\partial Y} \tag{15}$$

and a boundary layer variable, η, by

$$\eta = (U_e X)^{1/2} Z \tag{16}$$

Introduce two functions $f(X,Y,\eta)$ and $g(X,Y,\eta)$ where,

$$\psi = (U_e X)^{1/2} Xf \ , \qquad \phi = \left(\frac{X}{U_e}\right)^{1/2} V_e g \tag{17}$$

For conical inviscid flow, fluid properties do not vary along rays; therefore, for any flow parameter, H, $\partial H/\partial X = 0$. Then using eqs. (12), (16) and (17) in eq. (15), the following are obtained:

$$\frac{U}{U_e} = \frac{\partial f}{\partial \eta} = F(Y,\eta) \tag{18a}$$

$$\frac{V}{V_e} = \frac{\partial g}{\partial \eta} = G(Y,\eta) \tag{18b}$$

Equation (18) may be written as the vector equation,

$$\frac{\partial h}{\partial \eta} = H \tag{19}$$

where $h = \begin{bmatrix} f \\ g \end{bmatrix}$ and $H = \begin{bmatrix} F \\ G \end{bmatrix}$ (20)

With eqs. (12)-(20), eqs. (2) and (3) may be combined and written as,

$$\frac{\partial^2 H}{\partial \eta^2} + \sigma \frac{\partial H}{\partial \eta} + \frac{V_e}{U_e}\left(\frac{\partial g}{\partial Y}\ \frac{\partial H}{\partial \eta} - G \frac{\partial H}{\partial Y}\right) = \Gamma \tag{21}$$

where $\sigma = 1.5f + \beta g$ (22)

and $\Gamma = \begin{bmatrix} \beta_u(FG-1) \\ (FG-1) + \beta_v(G^2-1) \end{bmatrix}$ (23)

The boundary conditions for eqs. (19) and (21) are:

$$\eta = 0 : \quad h = H = \begin{bmatrix} 0 \\ 0 \end{bmatrix}, \qquad \eta = \eta_e : \quad H = \begin{bmatrix} 1 \\ 1 \end{bmatrix} \tag{24}$$

Equations (19) and (21) may be solved in the direct mode, using prescribed inviscid velocities, to calculate viscous properties such as skin-friction coefficients and integral thicknesses. However, in the inverse mode, the inviscid velocities are unknown functions and must therefore be eliminated from the left-hand side of eq. (21). This is accomplished through the additional transformation,

$$Y^* = \int_0^Y \left(\frac{U_e}{V_e}\right) dY \tag{25}$$

Using eq. (25) in eq. (21), the latter becomes,

$$\frac{\partial^2 H}{\partial \eta^2} + \sigma \frac{\partial H}{\partial \eta} + \frac{\partial g}{\partial Y^*} \frac{\partial H}{\partial \eta} - G \frac{\partial H}{\partial Y^*} = \Gamma \tag{26}$$

$$\text{where now,} \quad \beta_u = \frac{1}{U_e} \frac{dU_e}{dY^*}, \quad \beta_v = \frac{1}{V_e} \frac{dV_e}{dY^*} \tag{27}$$

Numerical Procedure

The governing equations are differenced using the half-implicit finite-difference scheme of Matsuno (ref. 17). The scheme is second-order accurate and unconditionally stable, and was demonstrated by Woodson and DeJarnette (ref. 18) to yield accurate numerical results when compared to the exact solution of the three-dimensional boundary layer equations for parabolic flow over a moving flat plate.

For fully three-dimensional problems the scheme has the advantage that the crossflow derivative formulas are formed independent of the direction of the cross-flow. Further, the scheme is non-iterative based on a predictor-corrector linearization, a convenient feature for inverse boundary layer methods. For any flow parameter, H, the notation $H_{j,k} = H(Y^*_j, \eta_k)$ is used where,

$$\begin{aligned} Y^*_{j+1} &= Y^*_j + \Delta Y^* , \qquad j = 1,2,\ldots,JMAX \\ \eta_{k+1} &= \eta_k + \Delta\eta , \qquad k = 1,2,\ldots,KMAX \end{aligned} \tag{28}$$

Central difference operators are defined by:

$$\Delta_\eta H_{j,k} = (Hj,k+1 - Hj,k-1)/\Delta\eta \tag{29}$$

$$\Delta_Y{}^*H_{j+1/2,k} = (H_{j+1,k} - H_{j,k})/\Delta Y^* \tag{30}$$

$$\delta_\eta H_{j,k-1/2} = (H_{j,k} - H_{j,k-1})/\Delta\eta \tag{31}$$

$$\delta_\eta^2 H_{j,k} = (H_{j,k+1} - 2H_{j,k} + H_{j,k-1})/\Delta\eta^2 \tag{32}$$

and a backward difference operator for the predictor stage by,

$$\nabla_Y{}^*H_{j+1/2,k} = 2(H_{j+1/2,k} - H_{j,k})/\Delta Y^* \tag{33}$$

With the operators defined above, eqs. (19) and (26) become at the predictor stage, respectively,

$$\delta_\eta h_{j+1/2,k-1/2} = (H_{j+1/2,k} + H_{j+1/2,k-1})/2 \tag{34}$$

$$\delta_\eta^2 H_{j+1/2,k} + \sigma_{j,k}\Delta_\eta H_{j,k} + \nabla_Y{}^*g_{j+1/2,k}\Delta_\eta H_{j,k} - G_{j,k}\nabla_Y{}^*H_{j+1/2,k} = \Gamma_{j,k} \tag{35}$$

at the corrector stage they are,

$$\delta_\eta h_{j+1,k-1/2} = (H_{j+1,k} + H_{j+1,k-1})/2 \tag{36}$$

$$\delta_\eta^2(H_{j+1,k} + H_{j,k})/2 + \sigma_{j+1/2,k}\Delta_\eta H_{j+1/2,k} + \Delta_Y{}^*g_{j+1/2,k}\Delta_\eta H_{j+1/2,k} - G_{j+1/2,k}\Delta_Y{}^*H_{j+1/2,k} = \Gamma_{j+1/2,k} \tag{37}$$

Equations (34)-(37) may be written in the block tridiagonal matrix form,

$$h_k = h_{k-1} + \frac{\Delta\eta}{2}(H_k + H_{k-1}) \tag{38a}$$

$$-H_{k-1} + B_k H_k - H_{k+1} + a_k h_k = D_k \tag{38b}$$

where a_k and B_k are 2x2 coefficient matrices and D_k is a vector. Equations (38) are linear tridiagonal matrix equations and may be solved using a block form of the Davis modified tridiagonal alogrithm (ref. 19).

The term D_k in eq. (38b) contains terms with both β_u and β_v as coefficients. However, in the inverse mode these parameters are unknowns which must be determined from the solution. Taking advantage of the fact that eq. (38) is linear, one may write,

$$D_k = D_k^{(0)} + \beta_u D_k^{(1)} + \beta_v D_k^{(2)} \tag{39a}$$

$$H_k = H_k^{(0)} + \beta_u H_k^{(1)} + \beta_v H_k^{(2)} \tag{39b}$$

and $$h_k = h_k^{(0)} + \beta_u h_k^{(1)} + \beta_v h_k^{(2)} \tag{39c}$$

where the unknowns β_u and β_v are given by eq. (27). The boundary conditions associated with eq. (39) are:

$$\text{at} \quad \eta = 0 : \quad h_1^{(i)} = H_1^{(i)} = 0 , \qquad i = 0,1,2$$

$$\text{and at} \quad \eta = \eta_e : \quad H_{KMAX}^{(0)} = 1 , \quad H_{KMAX}^{(i)} = 0 , \qquad i = 1,2 \tag{40}$$

Carrying out the operations of eqs. (29)-(33), one may equate like powers of β_u and β_v to obtain

$$h_k^{(i)} = h_{k-1}^{(i)} + \frac{\Delta\eta}{2}\left(H_k^{(i)} - H_{k-1}^{(i)}\right) , \qquad i = 0,1,2 \tag{41a}$$

$$- H_{k-1}^{(i)} + B_k H_k^{(i)} - H_{k+1}^{(i)} + a_k h_k^{(i)} = D_k^{(i)} , \qquad i = 0,1,2 \tag{41b}$$

This system of equations may be solved to obtain $h_k^{(i)}$ and $H_k^{(i)}$ for $i = 0,1,2$. The parameters U_e and V_e are then determined from either the specified wall shear stresses or integral thicknesses. A streamwise integral thickness is defined by,

$$\bar{\delta}_X^* = \int_0^\infty \left(1 - \frac{U}{U_e}\right) d\bar{z} \tag{42}$$

Using eqs. (16) and (18a) in eq. (42) and integrating gives,

$$DTX = \frac{\bar{\delta}_X^*}{\bar{x}} \sqrt{Re_x} = \eta_e - f(\eta_e) \tag{43a}$$

In a similar manner,

$$DTY = \frac{\bar{\delta}_{Y^*}^*}{\bar{x}} \sqrt{Re_x} = \eta_e - g(\eta_e) \tag{43b}$$

With eq. (39c), eq. (43) may be written as,

$$DTX = \eta_e - f_{KMAX}^{(0)} - \beta_u f_{KMAX}^{(1)} - \beta_v f_{KMAX}^{(2)} \tag{44a}$$

$$DTY = \eta_e - g_{KMAX}^{(0)} - \beta_u g_{KMAX}^{(1)} - \beta_v g_{KMAX}^{(2)} \tag{44b}$$

Equations (44a) and (44b) are solved to obtain β_u and β_v. Now, returning to eq. (27) and taking second-order differences about the point j+1/2,

$$\beta_u(U_{e_{j+1}} + U_{e_j}) = \frac{2}{\Delta Y^*}(U_{e_{j+1}} - U_{e_j})$$

Then it follows that

$$U_{e_{j+1}} = U_{e_j}\left(1 + \frac{2}{\beta_u \Delta Y^*}\right)/\left(1 - \frac{2}{\beta_u \Delta Y^*}\right) \tag{45a}$$

$$V_{e_{j+1}} = V_{e_j}\left(1 + \frac{2}{\beta_v \Delta Y^*}\right)/\left(1 - \frac{2}{\beta_v \Delta Y^*}\right) \tag{45b}$$

Next, consider if the wall shear were perscribed. The surface skin-friction coefficients are defined by

$$C_{f_X} = \bar{\nu}\left(\frac{\partial \bar{U}}{\partial \bar{z}}\right)_w / \frac{1}{2}\bar{U}_e^2 , \qquad C_{f_{Y^*}} = \bar{\nu}\left(\frac{\partial \bar{V}}{\partial \bar{z}}\right)_w / \frac{1}{2}\bar{U}_e \bar{V}_e \tag{46}$$

Using eq. (5) in eq. (46) one obtains,

$$CFX = C_{f_X} \sqrt{Re_x} = 2\left(\frac{\partial F}{\partial \eta}\right)_w \tag{47a}$$

$$CFY = C_{f_{Y^*}}\sqrt{Re_x} = 2\left(\frac{\partial G}{\partial \eta}\right)_w \tag{47b}$$

Using second-order accurate difference expressions for the derivatives in eq. (47) yields,

$$CFX = \frac{18F_2 - 9F_3 + 2F_4}{3\Delta\eta} \tag{48a}$$

$$CFY = \frac{18G_2 - 9G_3 + 2G_4}{3\Delta\eta} \tag{48b}$$

Substituting eq. (39b) into eq. (48) gives two equations for the two unknowns, β_u and β_v. An advantage of the present method over some earlier methods (refs. 4-6) is that the solution for β_u and β_v is obtained without column iteration, as opposed to using an under-relaxation scheme. For regions of reversed flow the FLARE approximation is made at the predictor stage,

$$G\frac{\partial H}{\partial Y^*} = 0 \tag{49a}$$

while at the corrector stage,

$$G\frac{\partial H}{\partial Y^*} = G_{j+1/2,k}\left(\frac{H_{j+1/2,k} - H_{j,k}}{\Delta Y^*/2}\right) \tag{49b}$$

Equation (49) insures diagonal dominance of the Davis modified algorithm in the reversed flow region. Note that eq. (49) reduces the accuracy of the finite-difference method to first order. Carter (ref. 5) added an artificial "time-like" term to the B_k term in eq. (38b) to ensure unconditional diagonal dominance in his solution algorithm. For the cases computed thus far, no instabilities were encountered in the reversed flow region when evaluating the convective derivatives according to eq. (49).

RESULTS AND DISCUSSION

Two-dimensional Flow

Calculations using the inverse boundary layer method are first discussed for flow over a circular cylinder. The inviscid solution for flow over a circular cylinder is given from potential theory by,

$$u_e = 2\sin\theta \tag{50}$$

where θ is the angle measured with respect to the x axis which defines the cylinder ($0 \leq \theta \leq \pi$). The boundary layer was computed in the direct mode until separation was encountered at $\theta = 104.5$ deg and then the calculations were continued in the inverse mode by specifying the skin-friction coefficient to be constant and equal to its value one marching step beyond separation (CFX = 0 or slightly negative). Let f in eq. (8) and F in eq. (9) be written as,

$$f_k = f_k^{(0)} + m f_k^{(1)} \tag{51a}$$

$$F_k = F_k^{(0)} + m F_k^{(1)} \tag{51b}$$

with corresponding boundary conditions,

$$\begin{aligned} &\text{at} \quad \eta = 0 : \; f_1^{(i)} = F_1^{(i)} = 0 , \quad i = 0,1 \\ &\text{and at} \quad \eta = \eta_e : \; F_{KMAX}^{(0)} = 1 , \quad F_{KMAX}^{(1)} = 0 \end{aligned} \tag{52}$$

After substituting eq. (51) into eq. (9), two separate equations result; one for the variables with superscript (0) and another for superscript (1). After solving these two equations, the value of m can be calculated by substituting eq. (51) into eq. (48a). The values of m can then be used to numerically calculate u_e at each marching station. The resulting edge velocity is shown in fig. 3. The edge velocity from the inverse calculation departs tangentially from the potential flow curve at the separation point and $\theta = \pi$ is no longer a stagnation point. The inverse method could be used to calculate the edge velocity over the entire cylinder provided the wall shear or displacement thickness distribution is known.

Klineberg and Steger (ref. 4) constructed a test case for a flow with separation and reattachment by prescribing the skin-friction distribution as,

$$\begin{aligned} &CFX = \frac{.664}{12}(X-2)(X-6) = \tau_1 , \quad X < 2, \; X > 6 \\ &CFX = \tau_1 [1 + \hat{\alpha}(X-2)(X-6)] , \quad 2 \leq X \leq 6 \end{aligned} \tag{53}$$

where $\hat{\alpha}$ is a given parameter. The resulting pressure gradient parameter, m, for $\hat{\alpha} = 0.225$ was calculated and is compared to that which was determined by Klineberg and Steger in fig. 4. Klineberg and Steger required between 400 to 800 iterations using a point successive-under-relaxation scheme for the calculation of m while the present results were obtained with one downstream pass. The corresponding displacement thickness and edge velocity for this case are given in fig. 5, and velocity profiles at three marching stations are shown in fig. 6. It was found that for

attached flow the profile for $F_k^{(1)}$ was primarily positive, while for separated flow the majority of the $F_k^{(1)}$ profiles were negative.

A second test case is that of Carter (ref. 5) in which the displacement thickness is perscribed according to the relation,

$$DTX = a_1 + a_2(X-X_o) + a_3(X-X_o)^2 + a_4(X-X_o)^3 \ , \quad X \leq X_o$$

$$DTX = \hat{a}_1 + \hat{a}_2(X-X_1) + \hat{a}_3(X-X_1)^2 + \hat{a}_4(X-X_1)^3 \ , \quad X_1 \leq X \leq X_2 \tag{54}$$

where $X_o = 1.065$, $X_1 = 1.35$, $X_2 = 1.884$ and the values of the a's are determined such that at $X = X_o$ the value and slope of the displacement thickness match the Blasius flat plate distribution, and at $X = X_1$, DTX reaches a maximum value. The case identified by Carter as Case B has a maximum displacement thickness of 8.6 and its distribution is presented in fig. 7a along with the resulting skin-friction distribution in fig. 7b. The calculated value of m for this case is compared with Carter's results in fig. 8a. Carter also developed an "approximate forward marching" technique in addition to his globally iterative method, which employs the FLARE approximaton. Both of his methods, however, used an under-relaxation scheme for the calculation of m. For the grid indicated in fig. 8, Carter's globally iterative scheme converged in 130 iterations and his forward marching procedure required an average of 41 column iterations at each marching step. The present method required only one downstream pass. The edge velocity is presented in fig. 8b.

This test case has a more extensive separated flow region than the Klineberg and Steger case with the approach to separation and reattachment much steeper. Note that m reaches a relative minimum just prior to separation and reattachment which satisfies Meksyn's criterion (ref. 20) for a regular solution. Velocity profiles at two x-locations are given in fig. 9. At the point $X = 1.393$, nearly half of the profile is in the reversed flow region, however, the magnitude of the reversed flow velocity is small compared to the edge value. For this test case, the maximum negative value of u is about one-tenth of u_e.

Conical Flow Over Delta Wings

The inviscid solution for the Hummel delta wing at 20.5 deg incidence was determined using the Free Vortex Sheet (FVS) theory (refs. 12-14). The FVS code solves the linearized Prandtl-Glauret equation for potential flow. It represents the wing, wake, and rolled-up vortex sheets by continuous quadratic doublet sheet distributions and the vortex core by a line distribution of vortices. Detailed pressure distributions as well as overall forces and moments are predictd by the FVS code; however, no effort is made to model the secondary vortices in the inviscid calculation.

The viscous calculations were begun in the direct mode beginning at the reattachment line (which was found to be located along the wing centerline for this case) and marched spanwise until the secondary separation line was encountered.

The secondary separation line is assumed to be the line along which CFY first goes through zero. The solution was then continued in the inverse mode by specifying the skin-friction coefficients to be constant and equal to their values at separation (CFY $\leq$ 0 but CFX > 0). The spanwise distribution of the skin-friction coefficients is presented in fig. 10a with corresponding integral thicknesses in 10b. The secondary separation line was calculated to be along Y = 0.70. Hummel (ref. 15) observed from oil flow studies a secondary separation line along Y = 0.67. A discrepancy between the calculated and observed secondary separation line was expected, since the inviscid solution ignores completely the influence of the secondary vortices. Reference 1 showed that the secondary separation line could be calculated accurately with the direct boundary layer method when experimental pressure data were used. The momentum integral thicknesses and shape factors are shown in fig. 11. Both shape factors increase sharply in the vicinity of the secondary separation line with the spanwise shape factor remaining nearly constant afterwards while the streamwise shape factor decreases continually toward the leading edge. Velocity profiles at three spanwise stations are presented in fig. 12. Both profiles indicate the spanwise thickening of the boundary layer and the G profiles beyond the secondary separation line show a small region of reversed flow near the surface. The inviscid velocities determined from the FVS code and those calculated with the inverse method are presented in fig. 13. As expected, the gradients in the inviscid velocities calculated from the inverse boundary layer method are much less steep than those of the inviscid solution calculated neglecting the boundary layer.

Research is in progress to interact the boundary layer solution with the inviscid solution. Reference 21 used a three-dimensional integral turbulent boundary layer method to solve the flow field over a delta wing at incidence. The viscous and inviscid solutions were coupled and the resulting pressure distribution showed some improvement over the inviscid results near secondary separation.

CONCLUDING REMARKS

A three-dimensional, direct boundary layer method was extended to the inverse mode for separated flows. It is a predictor-corrector finite-difference method in which the FLARE approximation is made to the streamwise momentum term in the preditor stage but a finite-difference quotient is used for the corrector stage. This method allows the inviscid velocity to be calculated without iterations by marching into the separated flow region using prescribed skin-friction coefficients or integral thicknesses.

Two-dimensional test cases for laminar separation with prescribed skin friction or displacement thickness were found to compare well with other methods. Solutions were also obtained using the direct and inverse modes for conical inviscid flow over a delta wing at incidence. The direct mode was used to the secondary separation line and then the inverse mode continued the solution into the separated flow region with both skin-friction coefficients maintained at their values at secondary separation. Further studies are needed for the inverse mode in fully three-dimensional flows and interacting the boundary layer solution with the inviscid solution.

SYMBOLS

a_k, B_k	coefficient matrices in eq. (38)
$C_{f_X}, C_{f_{Y^*}}$	skin-friction coefficients defined by eq. (46)
CFX,CFY	$C_{f_X}\sqrt{Re_x}$, $C_{f_{Y^*}}\sqrt{Re_x}$
D_k	vector in eq. (38)
DTX,DTY	$\frac{\bar{\delta}^*_X}{\bar{x}}\sqrt{Re_x}$, $\frac{\bar{\delta}^*_{Y^*}}{\bar{x}}\sqrt{Re_x}$
f,g	functions defined by eq. (17)
F,G	velocity ratios given by eq. (18)
H,h	vectors defined by eq. (20)
HX,HY	MTX/DTX, MTY/DTY
JMAX	number of mesh points in spanwise direction
KMAX	number of mesh points across the boundary layer
$\bar{L}$	reference length, m
m	parameter defined by eq. (10)
MTX,MTY	momentum integral thicknesses
Re	freestream Reynolds number, $\bar{U}_o\bar{L}/\bar{\nu}$
Re_x	local Reynolds number, $(U_eX)Re$
u,v,w	non-dimensional velocity components in x, y, and z directions, respectively
U,V,W	transformed velocity components given by eq. (13)
$\bar{U}_o$	freestream velocity, m/s
x,y,z	non-dimensional Cartesian coordinates streamwise, spanwise, and normal to the wing surface, respectively
X,Y,Z	transformed coordinates given by eq. (12)
Y*	transformed spanwise coordinate given by eq. (25)

$\hat{\alpha}$ parameter in eq. (53)

β_u $\frac{V_e}{U_e^2}\frac{dU_e}{dY}$

β_v $\frac{1}{U_e}\frac{dV_e}{dY}$

β $\beta_v - .5\beta_u$

Γ parameter defined by eq. (23)

δ central difference operators given by eqs. (31), (32)

$\bar{\delta}_X^*$ $\int_0^\infty \left(1 - \frac{\bar{U}}{U_e}\right)d\bar{z}$

$\bar{\delta}_Y^*$ $\int_0^\infty \left(1 - \frac{\bar{V}}{V_e}\right)d\bar{z}$

Δ central difference operators defined by eqs. (29), (30)

∇ backward difference operator defined by eq. (33)

η transformed normal coordinate defined by eqs. (5), (16)

θ angle of rotation for circular cylinder

Λ sweep angle of the delta wing

$\bar{\nu}$ kinematic viscosity coefficient, m^2/s

σ parameter defined by eq. (22)

ψ,ϕ stream functions given by eqs. (7), (15)

Subscripts

e edge value

j,k mesh point locations given by eq. (28)

v viscous calculation

w wall

Barred parameters are dimensional quantities.

REFERENCES

1. DeJarnette, F. R. and Woodson, S. H.: "Numerical and Experimental Determination of Secondary Separation on Delta Wings in Subsonic Flow," AIAA J. Aircraft, Vol. 22, No. 7, July 1985, pp. 602-608.

2. Catherall, D. and Mangler, K. W.: "The Integration of the Two-Dimensional Laminar Boundary-Layer Equations Past the Point of Vanishing Skin Friction," J. Fluid Mech., Vol. 26, Pt. 1, Sept. 1966, pp. 163-182.

3. Reyhner, T. A. and Flugge-Lotz, I.: "The Interaction of a Shock Wave with a Laminar Boundary Layer," Int. J. Non-Linear Mech., Vol. 3, No. 2, June 1968, pp. 173-199.

4. Klineberg, J. M. and Steger, J. L.: "On Laminar Boundary Layer Separation," AIAA Paper No. 74-94, Feb. 1974.

5. Carter, J. E.: "Inverse Solutions for Laminar Boundary-Layer Flows with Separation and Reattachment," NASA TR R-447, Nov. 1975.

6. Cebeci, T., Keller, H. B., and Williams, P. G.: "Separating Boundary-Layer Flow Calculations," J. of Comp. Physics, Vol. 31, 1979, pp. 363-378.

7. Le Balleur, J. C.: "Couplage visqueux-non visqueux: méthode numérique et applications aux écoulements bidimensinnels transsoniques et supersoniques," La Recherche Aérospatiale, Vol. 183, 1978, pp. 65-76.

8. Carter, J. E.: "A New Boundary-Layer Interaction Technique for Separated Flows," NASA TM 78690, June 1978.

9. Kwon, O. K. and Pletcher, R. H.: "Prediction of Incompressible Separated Boundary Layers Including Viscous-Inviscid Interaction," J. Fluids Eng., Vol. 101, Dec. 1979, pp. 466-472.

10. Veldman, A. E. P.: "New Quasi-Simultaneous Method to Calculate Interacting Boundary Layers," AIAA J., Vol. 19, No. 1, Jan. 1981, pp. 79-85.

11. Edwards, D. E. and Carter, J. E.: "Analysis of Three-Dimensional Separated Flow with the Boundary Layer Equations," AIAA Paper No. 85-1499, July 1985.

12. Johnson, F. T., Lu, P., Tinoco, E. N., and Epton, M. A.: "An Improved Panel Method for the Solution of Three-Dimensional Leading-Edge Vortex Flows, Volume I - Theory Document," NASA CR 3278, July 1980.

13. Luckring, J. M., Schoonover, W. E., and Frink, N. T.: "Recent Advances in Applying Free Vortex Sheet Theory for the Estimation of Vortex Flow Aerodynamics," AIAA Paper No. 82-0095, Jan. 1982.

14. Luckring, J. M., Hoffler, K. D, and Grantz, A. C.: "Recent Extensions to the Free-Vortex-Sheet Theory for Expanded Convergence Capability," Vortex Flow Aerodynamics - Volume I, NASA CP-2416, paper no. 4, 1986.

15. Hummel, D.: "Zur Umstromung scharfkantiger schlanker Deltaflugel bei grossen Anstellwinkeln," Zeitschrift fur Flugwissenschaften, Vol. 15, Oct. 1967, pp. 376-385.

16. Schlicting, H.: Boundary Layer Theory, McGraw-Hill Book Company, New York, NY, 1968.

17. Matsuno, L.: "A Vector-Orientated Finite-Difference Scheme for Calculating Three-Dimensinal Compressible Laminar and Turbulent Boundary Layers on Practical Wing Configurations," AIAA Paper No. 81-1020, 1981.

18. Woodson, S. H. and DeJarnette, F. R.: "A Three-Dimensional Boundary Layer Method for Flow over Delta Wings with Leading-Edge Separation," SAE Paper No. 851818 presented at the 1985 SAE Aerospace Technology Conference and Exposition, Long Beach, CA, Oct. 14-17, 1985.

19. Blottner, F. G.: "Introduction to Computational Techniques for Boundary Layers," Sandia Laboratories Report SAND - 79-0893, Albuquerque, New Mexico, 1979.

20. Meksyn, D.: New Methods in Laminar Boundary-Layer Theory, Pergamon Press, Inc., 1961.

21. Wai, J. C., Baillie, J. C., and Yoshihara, H: "Computation of Turbulent Separated Flows Over Wings," Third Symposium on Numerical and Physical Aspects of Aerodynamic Flows, Long Beach, CA, Jan. 21-24, 1985.

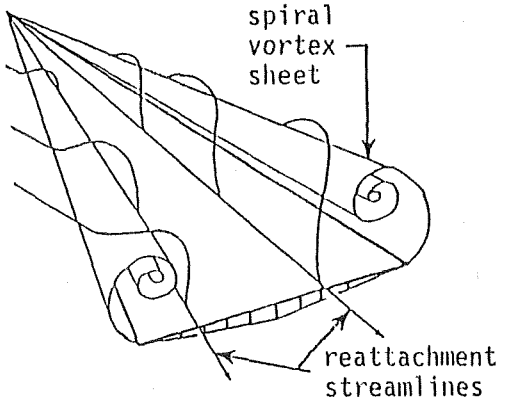

Fig. 1. Leading-edge vortex flow.

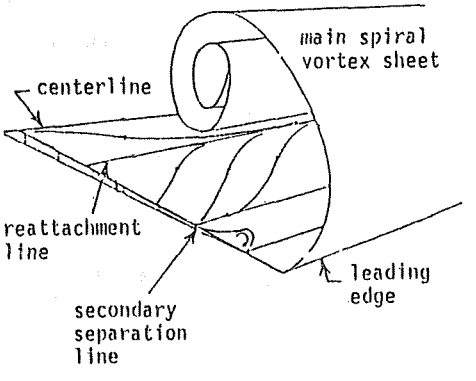

Fig. 2. Upper surface flow geometry.

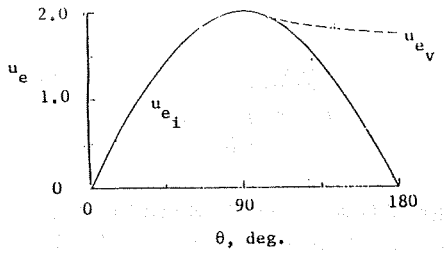

Fig. 3. Inviscid velocity over a circular cylinder.

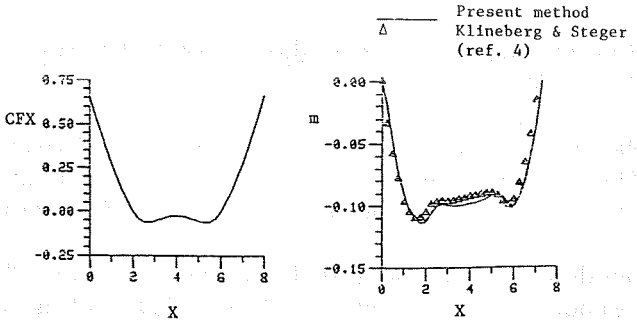

(a) (b)

Fig. 4. Skin-friction coefficient and pressure gradient parameter.

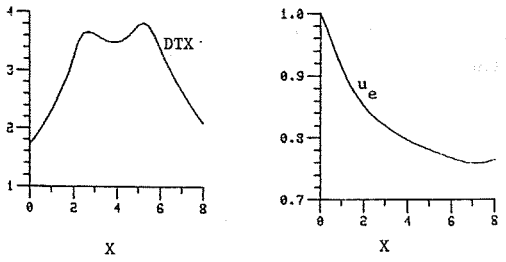

(a) (b)

Fig. 5. Displacement thickness and edge velocity.

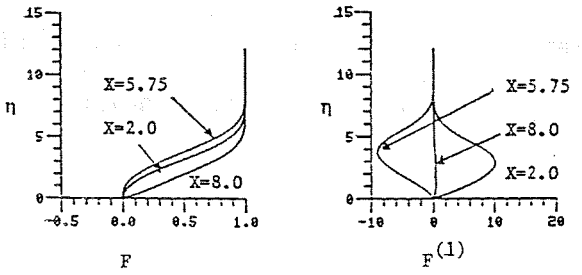

(a) (b)

Fig. 6. Velocity profiles for Klineberg and Steger test case.

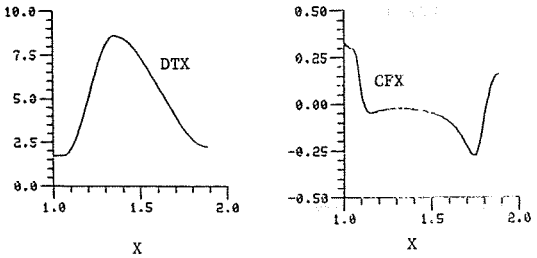

(a) (b)

Fig. 7. Displacement thickness and skin-friction coefficient.

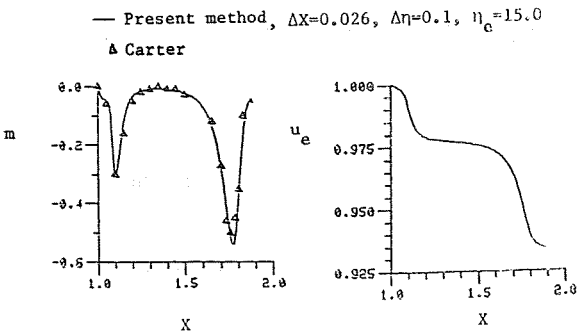

(a) (b)

Fig. 8. Pressure gradient parameter and edge velocity.

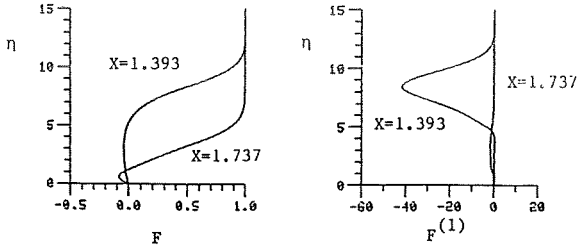

(a) (b)

Fig. 9. Velocity profiles for Carter test case.

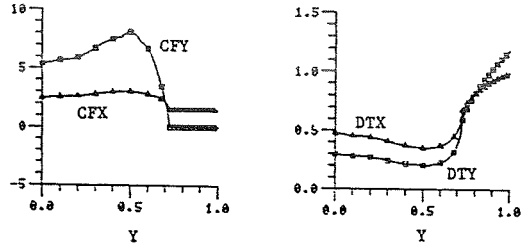

(a) (b)

Fig. 10. Skin-friction coefficients and integral thicknesses.

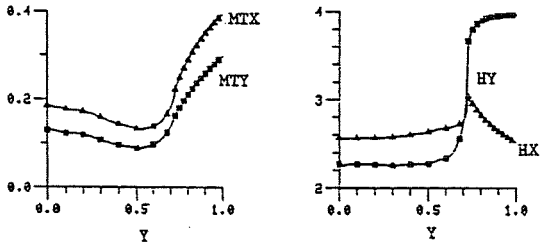

(a) (b)

Fig. 11. Momentum integral thicknesses and shape factors.

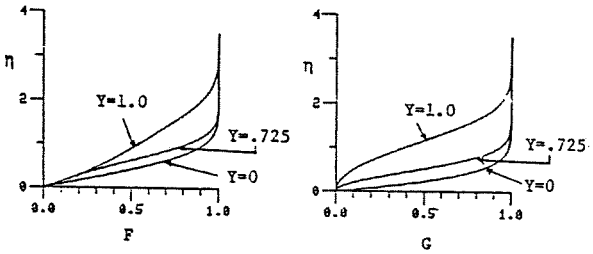

(a) (b)

Fig. 12. Velocity profiles for the delta wing.

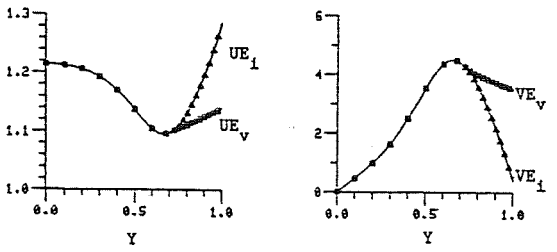

(a) (b)

Fig. 13. Inviscid velocity components.